Random Lasing with Systematic Threshold Behavior in Films of CdSe/CdS Core/Thick-Shell Colloidal Quantum Dots

Claudia Gollner,[†] Johannes Ziegler,[‡] Loredana Protesescu,[§,∥] Dmitry N. Dirin,[§,∥] Rainer T. Lechner,[⊥] Gerhard Fritz-Popovski,[⊥] Mykhailo Sytnyk,[†] Sergii Yakunin,[†,§,∥] Stefan Rotter,[¶] Amir Abbas Yousefi Amin,[#,▲] Cynthia Vidal,[‡] Calin Hrelescu,[‡] Thomas A. Klar,[‡] Maksym V. Kovalenko,[§,∥] and Wolfgang Heiss*[,†,#,▲]

[†]Institute of Semiconductor and Solid State Physics and [‡]Institute of Applied Physics, Johannes Kepler University Linz, Altenberger Straße 69, 4040 Linz, Austria, [§]Department of Chemistry and Applied Biosciences, ETH Zürich, Vladimir-Prelog-Weg 1, 8093 Zürich, Switzerland, [∥]Empa - Swiss Federal Laboratories for Materials Science and Technology, Uberlandstrasse 129, 8600 Dübendorf, Switzerland, [⊥]Institut für Physik, Montanuniversität Leoben, Franz-Josef-Strasse 18, A-8700 Leoben, Austria, [¶]Institute for Theoretical Physics, Vienna University of Technology, Wiedner Hauptstraße 8-10/136, 1040 Vienna, Austria, [#]Materials for Electronics and Energy Technology (i-MEET), Friedrich-Alexander-Universität Erlangen-Nürnberg, Martensstraße 7, 91058 Erlangen, Germany, and [▲]Energie Campus Nürnberg (EnCN), Fürther Straße 250, 90429 Nürnberg, Germany

ABSTRACT While over the past years the syntheses of colloidal quantum dots (CQDs) with core/shell structures were continuously improved to obtain highly efficient emission, it has remained a challenge to use them as active materials in laser devices. Here, we report random lasing at room temperature in films of CdSe/CdS CQDs with different core/shell band alignments and extra thick shells. Even though the lasing process is based on random scattering, we find systematic dependencies of the laser thresholds on morphology and laser spot size. To minimize laser thresholds, optimizing the film-forming properties of the CQDs, proven by small-angle X-ray scattering, was found to be more important than the optical parameters of the CQDs, such as biexciton lifetime and binding energy or fluorescence decay time. Furthermore, the observed systematic behavior turned out to be highly reproducible after storing the samples in air for more than 1 year. These highly reproducible systematic dependencies suggest that random lasing experiments are a valuable tool for testing nanocrystal materials, providing a direct and simple feedback for further development of colloidal gain materials toward lasing in continuous wave operation.

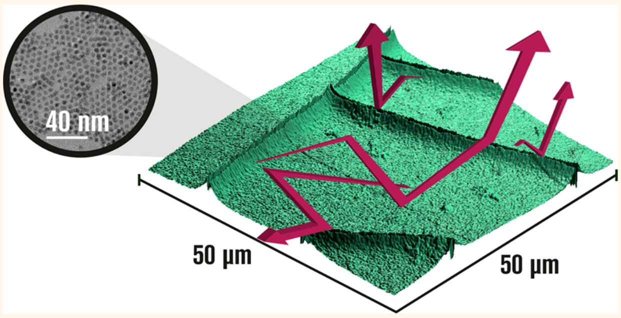

KEYWORDS: giant shell quantum dots · successive ion layer adsorption and reaction · random lasing · exciton–exciton interactions · plasmonics

Colloidal quantum dots (CQDs) based on CdSe nanocrystals covered by protective inorganic shells are an attractive material system due to their simple fabrication in solution, their size-adjustable optical properties, and their high environmental stability.[1−11] They also exhibit a preeminent photoluminescence (PL) quantum yield,[12−14] which suggested their use as nanophotonic light sources, for example, as fluorescence markers for biolabeling[15−19] and as active material in quantum-dot-based light-emitting diodes,[20−25] or to study the emission of single photons[26−28] in quantum-optical systems. In contrast to these applications based on spontaneous emission, CQDs exhibit severe drawbacks with respect to bulk semiconductors or nanoparticles of higher dimensionality (rods[29] and platelets[30,31]) in laser devices. This is because in CQDs the desired population inversion effectively dissipates by nonradiative Auger recombination, whose efficiency increases rapidly with decreasing dot radius r by $1/r^3$, and competes with the stimulated emission.[32−34] Thus, stimulated emission from CQDs is observed solely under intense, pulsed laser excitation. Contradictory statements are

* Address correspondence to wolfgang.heiss@fau.de.

Received for review May 6, 2015 and accepted September 12, 2015.

10.1021/acsnano.5b02739

reported concerning the optimum density of the CQDs in the gain material. While initial gain measurements were presented in dense CQD films,[35] laser emission has also been reported subsequently in droplets of diluted CQD solutions[36] or for a small number of CQDs dispersed on the surface of silica-based, toroidal microresonators.[37] Interestingly, for the latter case, record threshold energy densities have been achieved, which are about 3 orders of magnitude lower than those reported for the initial lasing experiments, performed on densely filled glass capillaries (at 77 K), used as ring resonators (see Table S1), even though similar CQD materials have been used. Significantly improved laser performance has been achieved by making use of especially designed core/shell nanoarchitectures with engineered exciton–exciton interactions, which were used to circumvent Auger recombination in CQDs due to exciton–exciton repulsion.[38] Thus, laser thresholds depend on a combination of material-related as well as CQD-specific parameters, which aggravates any systematic screening for optimized nanocrystal-based laser materials by measuring thresholds of individual laser devices.

Besides conventional lasers with judiciously engineered optical resonators, random lasers recently attracted a lot of attention, due to a set of appealing properties.[39−52] In random lasers, the optical feedback is provided by disorder-induced light scattering, for instance, achieved by mixing scattering particles into a laser-gain material.[43] In such mixtures, the light confinement is realized by the disorder scattering. The multiple scattering events involved in this process give rise to highly complex modes which can nevertheless result in narrow emission peaks.[43] Modal interactions through the gain medium in such lasers can be extremely strong, leading to a uniformly spaced frequency spectrum.[44] Random lasing is expected to have advantages in comparison to conventional lasing in illumination purposes as, for example, speckle-free images[50] using suitably designed random lasers with low spatial coherence. Controlling random lasers is a challenging problem on which, however, much progress has been reported recently.[39−41,45,47,53] Quantum-dot-based random lasing has already been observed in CdSe/ZnS core–shell CQDs, by depositing them on glass substrates with roughened grooves.[54] In this case, the rough surfaces of the grooves are considered to be important for enabling laser feedback, and a threshold fluence of 25 mJ/cm^2 is reported.

In this work, we present a systematic and thorough investigation of CQD-based random lasing, while an earlier report[54] only provides principle evidence that random lasing in CQDs is feasible. Our samples are uniform films of CdSe/CdS CQDs on planar glass substrates. By scanning the sample and recording laser thresholds at various positions, we find a systematic and highly reproducible relation between laser threshold and sample morphology, quantified in terms of stray light from the films under microscopic dark-field illumination, film roughness, degree of ordering of the CQDs in the films, and their density. The experiments were performed for core–shell CQDs with attractive as well as with repulsive exciton–exciton interactions. Even though the latter type exhibits in solution the most promising optical parameters (highest photoluminescence quantum yield, the longest biexciton decay time, and the longest exciton lifetime), we find for them in films laser thresholds higher than those for the CQDs with attractive exciton–exciton interactions. This highlights the important role of film morphology, which is influenced by other parameters such as CQD shape or amount of added ligands. Since the laser performance sensitively depends on all of these parameters, CQD-related and film-morphology-related ones, at the end, only lasing experiments are really suitable for selection of optimized materials for laser developments. While material evaluation by studying conventional laser devices is rather difficult, because the laser thresholds will be greatly affected by the choice of the used optical resonators, random lasing experiments might serve as a powerful tool for material selection because they provide reproducible dependencies on film morphology and laser spot size. These dependencies show essentially flat regions for laser spot sizes of >5×10^{-4} cm^2 and a film roughness of >600 nm, making this parameter range the most suitable for material evaluation, as shown below.

RESULTS AND DISCUSSION

To achieve population inversion, which is a prerequisite for the occurrence of laser emission, highly intense optical excitation is usually required,[35,36] which eventually causes damage to the nanocrystal materials. Therefore, in this study, highly emissive CdSe/CdS core–shell nanocrystals were used, which are protected by extra thick shells. In particular, three types were investigated, namely, (i) CdSe nanocrystals with a zinc blende structure and a shell of CdS grown by "successive ion layer adsorption and reaction" (SILAR),[4] whereby 8 layers were adsorbed (henceforth called SILAR I sample); (ii) CdSe nanocrystals as before, but with 15 monolayers of CdS (called SILAR II); and (iii) CdSe nanocrystals with wurtzite structure and a high-quality shell of CdS, grown by a slow co-injection of the Cd and S precursors, as was developed by Chen *et al.*[8] (this sample we call "co-inject" in the following; for the synthesis, see the Methods section, and for microscope images, see Figures S1 and S2). Here, both shell types were found to provide high environmental stability, so that all samples could be reproducibly measured while kept and stored in air. The CQDs SILAR I and SILAR II have a core diameter of 3.55 and 3.6 nm, respectively, and display different shell thicknesses, namely, 2.33 and 4.37 nm. These CQDs exhibit PL quantum yields of

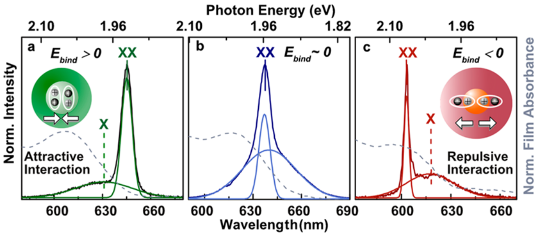

Figure 1. Amplified spontaneous emission. Under pulsed laser excitation and measured in stripe geometry, the CdSe/CdS core/thick-shell CQD films exhibit narrow emission peaks on top of the broader excitonic photoluminescence (X). The narrow peaks are caused by amplified spontaneous emission from biexcitons (XX). The wavelength shift between X and XX maxima is associated with the biexciton binding energy, E_{bind}, which is (a) >0, due to attractive exciton−exciton interactions in CQDs with type-I band alignment (sample SILAR I), and (c) <0 in type-II CQDs with repulsive X−X interaction (co-inject sample). In panel b (sample SILAR II), the exciton binding energy almost vanishes. In addition, the normalized film absorbance (gray dashed line) is presented. The 1S absorption maximum of the co-inject sample occurs at the ASE peak, counteracting stimulated emission.

44 and 53% in solution. For the co-inject CQDs with a core diameter of 3.1 nm and a shell thickness of 2.6 nm (Figure S2), an even higher quantum yield of 69% was found, which is typical for high-quality core/shell nanocrystal quantum dot materials.[2,3,8] As device structures for lasing experiments, thin nanocrystal films were deposited by doctor blade casting on glass substrates, which then act as two-dimensional (2D) optical waveguides. To evidence the lasing capability of both the nanocrystal materials and the films with thicknesses on the order of 1−2 μm, we first measured amplified spontaneous emission (ASE) in a stripe geometry.[55] Under pulsed excitation (532 nm, ~8 ps pulses), all studied CdSe/CdS CQDs exhibited a PL maximum close to 630 nm. Above a certain threshold, an additional narrow peak evolved, caused by amplified spontaneous emission (Figure 1a−c). While the PL is associated to single exciton (X) emission, the ASE is associated with emission from biexcitons (XX), evidencing a population inversion and gain in CQDs.[35] The ASE peak of the sample SILAR I is red-shifted with respect to the PL center by 43.5 meV (Figure 1a). This red shift indicates a positive biexciton binding energy, due to attractive exciton−exciton interactions, as is typically found in core/shell CQDs with a type-I band alignment.[38] In sample SILAR II, the ASE is found to be close to the center of the excitonic PL peak (Figure 1b), which is attributed to a biexciton with vanishing binding energy, indicative of a quasi-type-II band alignment between the core and shell material. Alternatively, the ASE peak on top of the PL maximum could also be ascribed to optical gain from the single excitons. In this case, according to Klimov *et al.*,[38] a second ASE peak should appear at higher pump intensities due to biexcitons. In our experiments, however, even up to the maximum available pump energies of 0.5 mJ, no such second peak could be observed. In addition, the threshold intensity for ASE for this sample was found to be close to that of SILAR I, for which the assignment of the ASE peak to biexcitons is not in question. Furthermore, transient pump−probe experiments confirmed this assignment, by exhibiting a biexponential decay due to a fast XX decay (134 and 202 ps biexciton decay times are found for SILAR I and SILAR II films, whereas longer times of 202 and 283 ps are measured in solution) and a much slower X recombination (Figure S3). Essentially, this interpretation is in agreement with Cihan *et al.*[56] In contrast to the SILAR samples, the co-inject sample (Figure 1c) exhibits a blue-shifted ASE peak. This blue-shifted ASE results from a repulsive exciton−exciton interaction, which is known to occur in core/shell CQDs with a type-II band alignment. The type II is considered to be beneficial with respect to Auger recombination, whose rate is reported to be reduced compared to that in type-I core/shell CQDs[57] (due to the charge separation between the core and shell material). Here we found indeed the longest biexciton decay times for the co-inject sample (270 ps in film and 470 ps in solution; Figure S3), making this sample the most promising for lasing experiments. Furthermore, the radiative lifetime of the single exciton should be prolonged, due to the reduced overlap between electron and hole wave functions. Indeed, in the co-inject sample, the X decay time is up to three times longer than that in the SILAR samples (τ_X = 19 ns is measured in films for co-inject, 13.8 ns for SILAR II, and 4.5 ns for SILAR I, Figure S4). Such an increase in lifetime for increasing charge separation is similar to those previously reported for type-I/type-II CQDs of CdTe/CdS or CdTe/CdSe[58] or of CdTe/ZnS,[59] and it again suggests that the co-inject material is the best for lasing experiments.

Random Lasing Supported by Plasmonic Gold Nanostars. The conventional approach toward random lasing is to immerse an arrangement of scattering particles into an optical gain material, where the particles provide the required optical feedback by causing multiple scattering events. Thus, in a first attempt to achieve random lasing in CQD films, we made use of gold nanoparticles, integrated into the wave-guiding SILAR I CQD film, similar to that reported previously.[60,61] To efficiently scatter the emission from the CQDs, the plasmon resonance of the gold nanoparticles needs to overlap with the CQD PL spectrum. Thus, we have chosen star-shaped gold nanoparticles that exhibit a broad extinction maximum at 647 nm due to Rayleigh scattering[62] close to the CQD's PL peak (Figure 2a). The ~100 nm large gold nanostars (Figure 2c) were deposited from a dilute solution on a glass substrate prior to the deposition of the CQD film to obtain a waveguide containing a random distribution of plasmonic scattering centers. These centers are clearly observed in the optical microscope image in Figure 2b, obtained under

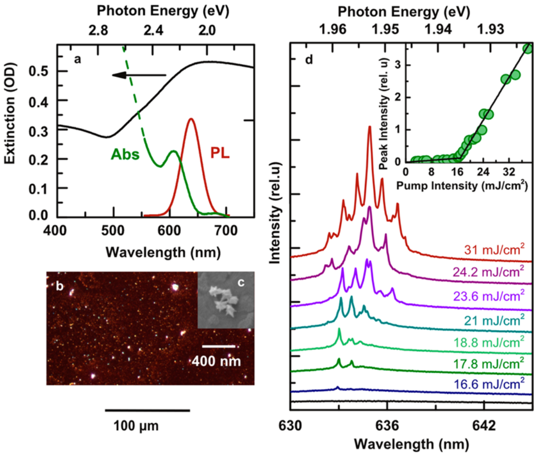

Figure 2. Random lasing due to scattering on gold nanostars. (a) Excitonic absorption peak and photoluminescence maximum of the SILAR I CdSe/CdS CQDs closely match the extinction maximum (black line) of the plasmonic gold nanostars in solution. (b) Dark-field optical microscope image of a SILAR I CQD film on top of a glass substrate covered by gold nanostars as scattering centers. (c) Electron microscopy image of five plasmonic nanostars. (d) Spectral evolution of the CQD emission with increasing pump intensity and the corresponding characteristic threshold behavior, deduced from the maxima of the PL spectra (inset).

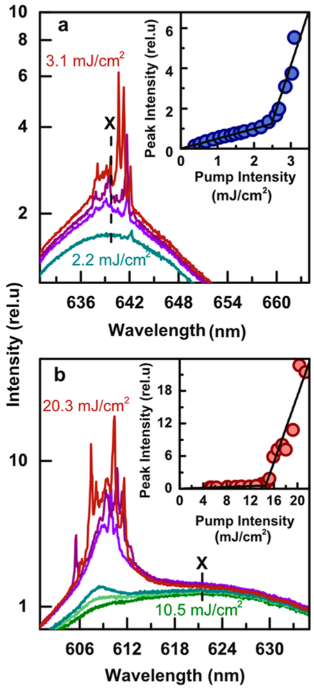

Figure 3. Random lasing with different spectral behavior. (a) SILAR II CQD films exhibit narrow laser modes just above the threshold intensity, whereas the giant shell film in (b) exhibits an amplified spontaneous emission spectrum above the threshold. This different behavior points toward a different scattering mechanism being responsible for the random lasing. Experiments were performed by <1.3 ns laser pulses with a repetition rate of 2500 Hz. The insets present characteristic threshold curves with threshold intensities of (a) 2.2 mJ/cm^2 and (b) 14.5 mJ/cm^2, measured with a size of the excitation spot of 3.1 × 10^{-4} cm^2 (r = 100 μm).

dark-field illumination. The CQD–gold nanostar composite film was excited by 1.3 ns laser pulses (532 nm, 100 Hz repetition rate), which were only moderately focused to a 200 μm diameter spot, to overcome a critical minimal gain volume.[43] The emission spectra, collected in backscattering geometry, exhibited unmistakable signatures of lasing behavior (Figure 2d). Narrow emission peaks appeared above a threshold intensity of 16.6 mJ/cm^2. With increasing intensity, the number of spectrally narrow laser modes increased, and for a pump intensity of 31 mJ/cm^2, a rather symmetrical emission spectrum was observed, with a spectral distance between the individual lasing modes of ∼0.7–0.9 nm and line widths around 0.3 nm. The threshold behavior is further evidenced by the kink in the dependence of the peak intensity as a function of the pumping intensity (the inset of Figure 2d shows the maximum amplitude of the PL spectra). Therefore, we conclude that our CQD films clearly show the hallmarks of a random laser.

Random Lasing from Pure CQD Films. The random lasing described above can be attributed to the feedback caused by multiple scattering events at the incorporated plasmonic gold nanostars. However, we also observed random lasing in CQD films that do not contain any additional scattering centers. In this case, any variation of the refractive index within the film waveguides causes the scattering that is required to provide an optical feedback. These variations can be weak and can be caused simply by slight variations of the film thickness, or these variations can be abrupt and caused by cracks or ridges in the film that are formed during evaporation of the solvent. Small-angle X-ray measurements (discussed below) also reveal some 3D ordering of the CQDs in the films (face-centered cubic lattice in the co-inject sample with finite dimensions), which indicates the presence of aggregates embedded in an otherwise unordered film. These aggregates also can act as scattering centers. As a result, a 25-fold higher repetition rate of the excitation laser (2.5 kHz instead of 100 Hz) could be used because the CdSe/CdS core/shell nanocrystals turned out to be substantially more stable under intense laser excitation than the gold nanostars. The latter showed the tendency to melt when more energy is deposited, due to the higher repetition rates. The pure CQD films also exhibited a clear lasing behavior, as is shown in Figures S5 for SILAR I CQDS and in Figure 3a for SILAR II CQDs. For both cases, the threshold intensity was similar and lower as compared to the value achieved with gold nanoparticle scattering. In Figure 3a, the lasing threshold is reached at a pump intensity of 2.2 mJ/cm^2, above which a first narrow mode appears at a wavelength of 642 nm, right in the center of the ASE spectrum of this sample (Figure 1b). When the pump intensity is further increased, additional lasing modes emerge, whose line widths (<0.2 nm) were limited by the spectrometer resolution. The modes

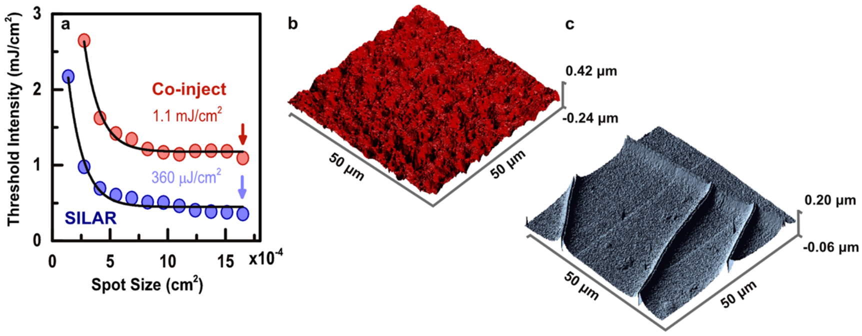

Figure 4. Threshold dependence on excitation spot size. (a) Both SILAR and co-inject sample types exhibit the expected exponential decrease of threshold intensity with increasing pump area (active volume). The sample providing the higher photoluminescence quantum yield (co-inject) exhibits the higher threshold intensity. AFM image of (b) co-inject sample and (c) SILAR sample, showing completely different film morphologies.

were rather stable, and their shift from subsequently taken spectra was in the range of their line width. This is shown in Figure S6a, exhibiting spectra collected for single excitation pulses (the data shown in Figures 2 and 3 are integrated over many excitation pulses). However, strong mode competition is observed, with increasing pump power; some modes became suppressed, whereas others became more pronounced (Figure 3). This can be ascribed to both the spectral and the spatial overlap of random laser modes.[44] The multimode spectrum observed in our samples also shows variations from shot to shot, corresponding to previous observations along the same lines.[63] The sensitivity with respect to a slight modification in the pump is clearly evidenced by the set of spectra measured for single pulse excitations (see Figure S6a). Further, the spacing between the modes was similarly pronounced, as in the case of the nanostar-supported random lasing (Figure 2d and Figure S5a).

In contrast, the random lasing in a film of the co-inject sample shows a different behavior (Figure 3b). In this case, just above the lasing threshold, the spectra do not exhibit individual narrow peaks but rather form a shape like the ones in the ASE measurements of the same sample (Figure 1c). Only at excitation intensities substantially higher than the threshold, individual modes appear in the spectra (which are integrated over many excitation pulses). Also, the spectra collected after single pulse excitation show a behavior slightly different than that for the SILAR I and II samples, in that the spectral positions of some of the modes vary from pulse to pulse, and the mode distances are rather irregular (Figure S6b). We attribute the spectral behavior of the co-inject sample showing the ASE-like laser spectra to a lack of spatial coherence, which indicates the origin of scattering to be different than that of the SILAR I and II samples. To unravel these differences, the surface morphology of the films was investigated by atomic force microscopy (AFM) (see Figure 4), and indeed, different film-forming properties were observed for the SILAR samples and the co-inject sample. While the co-inject sample exhibited a substantial film roughness and showed distinct pits with varying size and shapes spread all over the CQD film, the SILAR samples were much smoother and practically exhibited no pits. Instead, the SILAR films exhibited cracks and ridges, formed during solvent evaporation. Both the pits and the cracks (ridges) cause light scattering and thus may act as randomly formed resonators. We attribute the differences in the film morphology of the co-inject samples and the SILAR samples to the different CQD shapes and eventually to a different ligand coverage. The film morphology was studied in depth by grazing incidence small-angle X-ray scattering (GISAXS) measurements. Two-dimensional diffraction patterns were recorded slightly above the critical angle of around 0.3°, as calculated by assuming a homogeneous CdSe/CdS film. For all samples (reference samples on Si substrates were used, prepared identical to those used for the lasing experiments), several radial symmetric diffraction half-rings were observed, corresponding to powder-like ordering of crystalline domains (Figure S7). After azimuthal integration of the two-dimensional GISAXS pattern, we obtained 1D spectra, where the scattered intensity is plotted over the reciprocal scattering vector *Q* (symbols in Figure S8). The clearly visible diffraction peaks indicate the formation of ordered CQD aggregates. In this respect, the co-inject sample exhibits the highest degree of ordering because its 1D spectrum exhibits the most and strongest peaks. For a quantitative analysis, the 1D GISAXS spectra were fitted by a model, assuming aggregation of polydisperse hard spheres as described for nanocrystals,[68] with a close packing up to a volume fraction of 0.64. The model assumes that the form factor describing the scattering of the individual particles $P(Q)$ and the structure factor $S(Q)$, which describes the influence by particle arrangement, can be separated.[69] We derived as a one-fit parameter the total volume fraction, which includes the inorganic QDs together with their surrounding ligands. For all three samples, a value close to 0.64, which is the maximum value for fractal aggregates, was found, indicating that the CQD films are close to a crystalline ordered lattice. The main result of this fit procedure, which excellently describes the data in Figure S8, is the separated pair distance distribution functions $p(r)$ and the structure factors $S(Q)$, as shown in Figure S9. While the first function provides information about the maximum inorganic particle dimensions (8, 14, and 10 nm are deduced for SILAR I, SILAR II, and co-inject, respectively) and particle shapes, the second provides the mean particle separation including inorganic CQD diameter and organic ligand length. Dividing the deduced inorganic particle volume by the total particle volume (inorganic plus ligands), we calculated the inorganic CQD contribution to the total volume fraction, which is very high in the case of sample SILAR II (90%), moderately high for SILAR I (70%), and substantially lower for the co-inject sample. For the latter, dependent on the assumed particle shapes, values for the inorganic volume contribution between 9% (tetrahedral pyramides) and 50% (spherically shaped analogues) are obtained. The combination of high ordering and low inorganic volume fraction in the films of the co-inject sample indicates that the CQDs form aggregates which are separated by excess organic ligands. This is in agreement with the different surface topography observed by the AFM and will also affect the lasing properties of the thin film samples.

Threshold Dependence on Film Morphology. A typical feature of random lasing is a strong dependence of the laser threshold on the size of the pump spot.[43] This is caused by the increase of the return probability of the propagating light, with increasing excitation area. In Figure 4a, the threshold intensity with respect to the pump spot size is reported for both sample types SILAR I and co-inject (SILAR II is omitted in the following discussion because it essentially provides the same threshold powers as SILAR I). The measurement was performed with a stripe-shaped excitation, whose length was gradually decreased, and the threshold behavior measured. The theory predicts an exponential decrease of the threshold intensity for an increase of the amplification volume,[43] which is in good agreement with our results. Furthermore, we find a systematically higher threshold power for the co-inject sample than for the SILAR sample. Taking into account the optical properties of the CQDs only, we describe above the biexcitonic and excitonic properties, the higher threshold power for the co-inject sample is rather surprising because it exhibits the best optical properties for lasing among the three studied sample types. This observation underlines that the morphological properties of the films are also important for the random lasing behavior. An obvious morphological reason for the higher threshold in the co-inject sample is the smaller volume fraction of the pyramidal-shaped co-inject CQDs in the film, which was deduced by the small-angle X-ray measurements described above to be substantially lower than those of the SILAR samples. Another reason might be the blue-shifted XX emission with respect to the PL peak because the biexciton emission is overlapping more with the absorption band of the single excitons than in the case of the type-I band alignment (SILAR I). The higher threshold in the co-inject sample we found also to be consistent with the analysis of the mean distance (the mean length that the laser light travels in the film before it is scattered out from the waveguide and leaves the sample). This length is deduced from averaged fast Fourier transformation (FFT) of laser spectra, excited under single pulse excitation. For the co-inject sample, this length was found to be substantially shorter than that for the SILAR I and SILAR II samples (80 ± 20 μm for co-inject sample *versus* 108 ± 7 and 114 ± 20 μm for the SILAR samples, Figures S10−S12), resulting in higher threshold powers according to laser theory. For the SILAR I sample, an outstanding low threshold intensity of 360 $\mu J/cm^2$ was observed for an excitation spot size of 55 μm × 3 mm, corresponding to a power density of 185 kW/cm^2. This value represents, to the best of our knowledge, the lowest threshold observed for any random laser based on a CQD material (see Table S1).

As highlighted above, the surface morphology of the films plays an important role in random lasing, and in fact, it has an important influence on the threshold intensity. To find relations between surface morphology and lasing properties, substrates with metallic markers were used. The markers allowed circular laser spots to be adjusted with a diameter of 200 μm with an accuracy of ∼1/10 of its diameter to predefined positions on the substrates. To quantitatively compare the morphology of the film at different positions on the substrate, the samples were inspected by dark-field optical microscopy. As in the case of the gold nanostars in Figure 2c, the dark-field images unraveled the features and defects in the film that were chiefly responsible for the scattering. For the low threshold SILAR II sample, the most substantial scattering was provided by cracks (ridges) in the films (Figure 5a). Film roughness also contributed to the scattered light intensity, which was observed as colored areas between the cracks. To make these observations more quantitative, the scattered light spectrum, integrated over the whole area of the image, was measured for all positions of interest on the sample under identical conditions. The spatially integrated dark-field spectra are shown in Figure 5b for the two dark-field images (rectangles POS I and POS II) shown in Figure 5a. They show stray light from two contributions: (i) from the white light illumination lamp and (ii) from the luminescence excited in the film by the lamp. The latter causes the peak at ∼630 nm wavelength, while the first is seen as the background whose intensity increases with increasing wavelength. Under laser excitation, both positions shown in Figure 5a exhibit

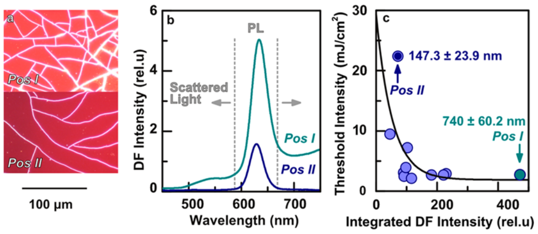

Figure 5. Systematic dependence of threshold intensity on film morphology. (a) Dark-field optical microscopy images of two positions on a film of SILAR II CQDs. Cracks contribute greatly to the scattered light intensity. Film roughness also affects scattered light and causes the films to appear in different brightness and color. (b) Spectral dependence of the scattered light, spatially integrated over the two rectangles POS I and POS II shown in (a). The peak at ∼630 nm is caused by luminescence, excited by the lamp. (c) Threshold intensity of numerous positions on the film, plotted against their corresponding spectrally integrated dark-field intensity. The laser threshold intensity decreases with increasing intensity of the scattered light. The data are fitted by an exponential decay. The numbers at the data points of POS I and POS II give the route mean square surface roughness measured at these positions.

random lasing, however, with substantially different laser thresholds of 22.5 and 2.7 mJ/cm^2 measured at POS II and POS I, respectively. Further positions on the sample provided threshold values between these two extremes. By spectrally integrating the dark-field spectra from 400 to 800 nm, we obained a value for the intensity that allows ordering of the obtained threshold values. The result, as shown in Figure 5c, is a systematic decrease of the laser threshold with increasing dark-field intensity. Thus, film morphologies providing intense scattering are beneficial for random lasing, whereas positions were also found where no lasing could be observed. These positions appeared rather dark in the dark-field images and were checked by AFM and exhibited minimal surface roughness of <20 nm (Figures S13). Interestingly, the random lasing behavior that we found turned out to be highly reproducible. The data in Figure S14 were taken for SILAR II, after the sample was stored for more than 1 year in air. We find a functional dependence of the laser threshold with respect to dark-field intensity that is the same as that in our initial experiments, and even the value for the threshold power, measured for high dark-field intensities (POS I), was almost identical to that measured 1 year before. Repeating the measurements several times by misaligning and aligning the excitation spot to the various positions on the samples allowed us to obtain the same results with small variations, which are expressed as error bars in Figure S14. This high reproducibility of the data justifies also providing the laser thresholds as a function of a more quantitative parameter as is given by the integrated dark-field intensity provided in relative units. Thus, we systematically studied the surface roughness of all investigated sample positions by high-resolution scanning confocal microscopy (examples of several positions are shown in Figure S15, providing similar images but different surface roughness ranging between *ca.* 50 and 750 nm). Roughly, the route mean square surface roughness scales linearly with the integrated dark-field intensity (Figures S16). Thus, the dependence of the random lasing thresholds as a function of surface roughness (Figure S17) also exhibits a functional dependence analogous to the laser thresholds as a function of integrated dark-field intensity shown in Figure 5c. From Figure S17, however, it becomes evident that, to compare results of different materials, sample positions with surface roughness larger than 600 nm should be chosen because in this range the functional dependence on roughness is rather flat and is thus insensitive to topographic details of the sample surface.

CONCLUSION

CdSe/CdS CQDs with especially thick shells are superior compared to standard core/shell CQD materials with respect to their environmental stability and due to the possibility to control the type of their band alignment. Here, three types of CdSe/CdS core/thick-shell materials have been investigated: two samples fabricated with the SILAR technique and different shell thicknesses and one grown by a co-injection method. Under pulsed laser excitation, we observed amplified spontaneous emission and random lasing from biexcitons, enabled by scattering, which provided the required optical feedback. Externally introduced plasmonic gold nanoparticles and cracks in the films were found to act as chaotically shaped resonators, providing rather stable mode patterns. Film roughness and pits caused rather extended modes, which we observed as broad-band, rather ASE-like spectra when they were integrated over many excitation pulses. Even though the optical feedback required for lasing was random scattering, some systematics in the threshold intensities were observed: (i) for sufficiently large excitation spots, the thresholds become insensitive to spot size; and (ii) minimal thresholds are obtained for films exhibiting strong scattering. Overall, morphological properties and the volume fractions of the inorganic CQDs in the films turned out to be at least as important, or even more important, to achieve low thresholds as the CQDs' optical properties. Thus, for material selection, only lasing experiments are finally conclusive, in contrast to studies of excitonic or biexcitonic properties which ignore the possible influence of morphology. The simplicity of the random lasing experiment, performed here at room temperature and with nanosecond long excitation pulses on films deposited on planar substrates, suggests that this technique is a simple and reliable standard tool to quantitatively evaluate CQDs for lasing purposes. Such a tool would be beneficial for material selection and optimization, without the need for fabricating elaborate devices or performing laborious experiments. Furthermore, in nonuniform materials, such as CQD films, the random lasing also impacts the properties of conventional lasing with external optical resonators, as was evidenced in the literature for epitaxially grown structures.[64] Thus, material development for lasing purposes—various different nanoarchitectures such as nanoplatelets, dot in rods, and nanowires are currently investigated—could be speeded up significantly to obtain nanolasers with continuous mode operation or also with potentially electrical excitation.

METHODS

Synthesis of SILAR CdSe/CdS CQDs. CdSe core NCs were synthesized following the established procedure described in ref 65. The precursors for the alternative injections, Cd-oleate in octadecene (ODE, 0.1 M) and S-ODE (0.1M), were prepared in advance and stored under argon. The shells of the nanocrystals were prepared according to ref 4. A 100 mL flask was loaded with 40 mg of CdSe (3.6 nm) dissolved in 1 mL of hexane, 2 mL of oleylamine, and 5 mL of ODE. The mixture was kept for 1 h under vacuum at 100 °C. After being switched to argon, the Cd precursor was injected and the temperature was increased to 240 °C. After 10 min, the S-precursor was injected. Every 10 min, successive injections were done to grow shells with nominal thicknesses of 8 layers (SILAR I) or 15 layers (SILAR II) of CdS. To account for the increasing diameter of NCs, the precursor volume for the first injection was 0.15 mL (0.1 M concentration), 0.76 mL for the eighth layer, and 1.32 mL for the 15th layer. After the last injection was finished, the flask was cooled and the NCs were washed with toluene and ethanol three times and finally redispersed in 1 mL of toluene.

Synthesis of Co-inject CdSe/CdS CQDs. Here, the two-step approach reported by Chen *et al.*[8] was used with minor modification. For the synthesis of wurtzite CdSe NCs, 30 mg (0.234 mmol) of CdO, 140 mg (0.418 mmol) of octadecylphosphonic acid (ODPA), and 1.5 g of trioctylphosphine oxide (TOPO) were mixed and degassed under Schlenk line vacuum for 1 h at 150 °C. Under nitrogen flow, the mixture was heated to 320 °C until a clear colorless solution formed and 0.5 mL of trioctylphosphine (TOP) was added. Then the reaction mixture was heated further to 370 °C; the heating source was removed, and a TOPSe/TOP (30 mg of Se in 0.25 mL of TOP) solution was swiftly injected. After 10 min, growth the reaction was terminated by fast cooling to room temperature. The resulting CdSe NCs were washed three times with acetone/hexane, redispersed in hexane, and filtered through a 0.2 μm filter. The size and concentration of the NCs were estimated by the position and amplitude of the excitonic absorption maximum, by making use of the calibration reported in ref 66. For growth of the CdS shell, a precursor solution of 1.56 mmol cadmium oleate in 6 mL of ODE and 81.8 μmol of hexanethiol in 6 mL of ODE was prepared and degassed. The cadmium oleate solution in ODE was prepared by heating CdO and oleic acid (1:2) in ODE up to 120 °C for 1 h. Then, 100 nmol of CdSe NCs was mixed with 3 mL of ODE and 3 mL of oleylamine (OLA) and degassed for 1 h at room temperature and 15 min at 120 °C. Under nitrogen flow, the reaction solution was heated to 310 °C at the rate of ~20 °C/min. When the temperature reached 240 °C, slow injection of precursor solutions started at the rate of 3 mL/h. After 2 h, 1 mL of oleic acid was injected and the solution was further annealed at 310 °C for 1 h. The resulting NCs were washed with ethanol/hexane, redissolved in hexane, and filtered through a 0.2 μm filter.

Synthesis of Gold Nanoparticles. The gold nanostars were synthesized by a seed-mediated growth and silver(I)-assisted synthesis method in aqueous solution using cetyltrimethyl ammonium bromide as the capping agent, similar to that reported in ref 67, but using only ascorbic acid as the reducing agent but no HCl, which results in a high yield of stars.

Film Preparation. The CQDs were deposited on glass substrates, which were cleaned by organic solvents in an ultrasonic bath and further treated by plasma cleaning and doctor blade casting (60 °C substrate temperature). Prior to the deposition, a series of markers was fabricated on the substrate by optical lithography followed by sputtering of 50 nm Pt.

Amplified Spontaneous Emission Measurements. For excitation, 8 ps laser pulses from a frequency-doubled Nd:YAG laser (time bandwidth, 532 nm, 10 kHz repetition rate) were focused by a cylindrical lens to provide a stripe on the sample. The luminescence was collected *via* the edge of the sample and detected by an AvaSpec-2048 spectrometer.

Random Lasing Experiments. Unless stated differently in the text, the samples were excited by <1.3 ns long laser pulses from a passively Q-switched solid-state laser (CryLas GmbH, 532 nm, repetition rates of 100 and 2500 Hz were used), moderately focused to a spot of ~200 μm diameter. The emission was collected in back-scattering geometry and detected by a grating spectrometer equipped with a CCD. Unless explicitly stated differently, spectra which were integrated over many excitation pulses are presented in the article. Spectra obtained for single excitation pulses were used to determine the mean distance $\langle d \rangle$. For this purpose, multiple emission spectra expressed as a function of wave vector in k space were Fourier transformed. The $\langle d \rangle$ is calculated by integral averaging ($\langle d \rangle = \mathrm{Int}[\mathrm{FFT}(x)*x]\mathrm{d}x/\mathrm{Int}[\mathrm{FFT}(x)]\mathrm{d}x$), and it is related to the optical mean path length $\langle L \rangle = \mathrm{PI}*\langle d \rangle/n$, with the refractive index of the material n.

Dark-Field Images and Spectra. The dark-field images were taken with an Olympus optical microscope, equipped with a camera and connected to a spectrometer. A white Anodisc 13 membrane disc was used as a reference, providing uniform scattering for white light.

Morphological Investigations. We have investigated the CQD layers on a Si substrate using a GISAXS setup at the Bruker Nanostar lab source to reveal the order of the CdSe/CdS–NC superlattices. The 2D patterns were recorded using a 2D detector (Vantec 2K) slightly above the critical angle of around 0.3°. The grazing angle of about 0.5° results in a footprint on the sample of about 0.3×5 mm^2, which allows probing a rather large sample volume. By azimuthal integration of the 2D GISAXS patterns, 1D plots were obtained, where the scattered intensity is plotted over the reciprocal scattering vector Q. The data were fit by a model, included in the GIFT software package,[68] based on the aggregation of polydisperse hard spheres with a close packing up to a volume fraction of 0.64. The direct particle interactions were described by means of the analytical Percus–Yevick approximation.[68] Noncontact three-dimensional surface topography studies were performed by making use of a μsurf confocal microscope (NanoFocus) with a lateral/vertical resolution of 300/2 nm, respectively.

Conflict of Interest: The authors declare no competing financial interest.

Supporting Information Available: The Supporting Information is available free of charge on the ACS Publications website at DOI: 10.1021/acsnano.5b02739.

Table S1 and Figures S1–S17 (PDF)

Acknowledgment. We thank the Austrian Science Fund FWF for funding through project F25 SFB-IR-ON. M.K. acknowledges financial support from European Union (FP7 ERC Starting Grant 2012, GA No. 306733) and from Swiss National Science Foundation (project 200021_143638); D.D. was funded by European Union *via* a Marie Curie Fellowship (PIIF-GA-2012-330524). J.Z., C.V., and T.A.K. acknowledge funding by the European Research Council (ERC) *via* Starting Grant "ActiveNP" (257158). R.T.L. acknowledges support by COMET/K2 centre MPPE.

REFERENCES AND NOTES

1. Hines, M. A.; Guyot-Sionnest, P. Synthesis and Characterization of Strongly Luminescing ZnS-Capped CdSe Nanocrystals. *J. Phys. Chem.* **1996**, *100*, 468–471.
2. Peng, X.; Schlamp, M. C.; Kadavanich, A. V.; Alivisatos, A. P. Epitaxial Growth of Highly Luminescent CdSe/CdS Core/Shell Nanocrystals with Photostability and Electronic Accessibility. *J. Am. Chem. Soc.* **1997**, *119*, 7019–7029.
3. Talapin, D. V.; Rogach, A. L.; Kornowski, A.; Haase, M.; Weller, H. Highly Luminescent Monodisperse CdSe and CdSe/ZnS Nanocrystals Synthesized in a Hexadecylamine−Trioctylphosphine Oxide−Trioctylphospine Mixture. *Nano Lett.* **2001**, *1*, 207–211.
4. Li, J. J.; Wang, Y. A.; Guo, W.; Keay, J. C.; Mishima, T. D.; Johnson, M. B.; Peng, X. Large-Scale Synthesis of Nearly Monodisperse CdSe/CdS Core/Shell Nanocrystals Using Air-Stable Reagents via Successive Ion Layer Adsorption and Reaction. *J. Am. Chem. Soc.* **2003**, *125*, 12567–12575.
5. Reiss, P.; Bleuse, J.; Pron, A. Highly Luminescent CdSe/ZnSe Core/Shell Nanocrystals of Low Size Dispersion. *Nano Lett.* **2002**, *2*, 781–784.
6. Xie, R.; Kolb, U.; Li, J.; Basché, T.; Mews, A. Synthesis and Characterization of Highly Luminescent CdSe−Core CdS/Zn0.5Cd0.5S/ZnS Multishell Nanocrystals. *J. Am. Chem. Soc.* **2005**, *127*, 7480–7488.
7. Mekis, I.; Talapin, D. V.; Kornowski, A.; Haase, M.; Weller, H. One-Pot Synthesis of Highly Luminescent CdSe/CdS Core−Shell Nanocrystals via Organometallic and "Greener" Chemical Approaches†. *J. Phys. Chem. B* **2003**, *107*, 7454–7462.
8. Chen, O.; Zhao, J.; Chauhan, V. P.; Cui, J.; Wong, C.; Harris, D. K.; Wei, H.; Han, H.-S.; Fukumura, D.; Jain, R. K.; Bawendi, M. G. Compact high-quality CdSe−CdS Core−Shell Nanocrystals with Narrow Emission Linewidths and Suppressed Blinking. *Nat. Mater.* **2013**, *12*, 445–451.
9. Htoon, H.; Malko, A. V.; Bussian, D.; Vela, J.; Chen, Y.; Hollingsworth, J. A.; Klimov, V. I. Highly Emissive Multiexcitons in Steady-State Photoluminescence of Individual "Giant" CdSe/CdS Core/Shell Nanocrystals. *Nano Lett.* **2010**, *10*, 2401–2407.
10. Vela, J.; Htoon, H.; Chen, Y.; Park, Y.-S.; Ghosh, Y.; Goodwin, P. M.; Werner, J. H.; Wells, N. P.; Casson, J. L.; Hollingsworth, J. A. Effect of Shell Thickness and Composition on Blinking Suppression and the Blinking Mechanism in 'Giant' CdSe/CdS Nanocrystal Quantum Dots. *J. Biophotonics* **2010**, *3*, 706–717.
11. Christodoulou, S.; Vaccaro, G.; Pinchetti, V.; De Donato, F.; Grim, J. Q.; Casu, A.; Genovese, A.; Vicidomini, G.; Diaspro, A.; Brovelli, S.; et al. Synthesis of Highly Luminescent Wurtzite CdSe/CdS Giant-Shell Nanocrystals Using a Fast Continuous Injection Route. *J. Mater. Chem. C* **2014**, *2*, 3439–3447.
12. Park, Y. S.; Malko, A. V.; Vela, J.; Chen, Y.; Ghosh, Y.; García-Santamaría, F.; Hollingsworth, J. A.; Klimov, V. I.; Htoon, H. Near-Unity Quantum Yields of Biexciton Emission from CdSe\CdS Nanocrystals Measured Using Single-Particle Spectroscopy. *Phys. Rev. Lett.* **2011**, *106*, 187401.
13. Greytak, A. B.; Allen, P. M.; Liu, W.; Zhao, J.; Young, E. R.; Popovic, Z.; Walker, B. J.; Nocera, D. G.; Bawendi, M. G. Alternating Layer Addition Approach to CdSe/CdS Core/Shell Quantum Dots with Near-Unity Quantum Yield and High On-Time Fractions. *Chem. Sci.* **2012**, *3*, 2028–2034.
14. Grabolle, M.; Ziegler, J.; Merkulov, A.; Nann, T.; Resch-Genger, U. Stability and Fluorescence Quantum Yield of CdSe−ZnS Quantum Dots—Influence of the Thickness of the ZnS Shell. *Ann. N. Y. Acad. Sci.* **2008**, *1130*, 235–241.
15. Bruchez, M.; Moronne, M.; Gin, P.; Weiss, S.; Alivisatos, A. P. Semiconductor Nanocrystals as Fluorescent Biological Labels. *Science* **1998**, *281*, 2013–2016.
16. Medintz, I. L.; Uyeda, H. T.; Goldman, E. R.; Mattoussi, H. Quantum Dot Bioconjugates for Imaging, Labelling and Sensing. *Nat. Mater.* **2005**, *4*, 435–446.
17. Wu, X.; Liu, H.; Liu, J.; Haley, K. N.; Treadway, J. A.; Larson, J. P.; Ge, N.; Peale, F.; Bruchez, M. P. Immunofluorescent Labeling of Cancer Marker Her2 and Other Cellular Targets with Semiconductor Quantum Dots. *Nat. Biotechnol.* **2003**, *21*, 41–46.
18. Resch-Genger, U.; Grabolle, M.; Cavaliere-Jaricot, S.; Nitschke, R.; Nann, T. Quantum Dots Versus Organic Dyes as Fluorescent Labels. *Nat. Methods* **2008**, *5*, 763–775.
19. Parak, W. J.; Pellegrino, T.; Plank, C. Labelling of Cells with Quantum Dots. *Nanotechnology* **2005**, *16*, R9.
20. Schlamp, M. C.; Peng, X.; Alivisatos, A. P. Improved Efficiencies in Light Emitting Diodes Made with CdSe(CdS) Core/Shell Type Nanocrystals and a Semiconducting Polymer. *J. Appl. Phys.* **1997**, *82*, 5837–5842.
21. Sun, Q.; Wang, Y. A.; Li, L. S.; Wang, D.; Zhu, T.; Xu, J.; Yang, C.; Li, Y. Bright, Multicoloured Light-Emitting Diodes Based on Quantum Dots. *Nat. Photonics* **2007**, *1*, 717–722.
22. Caruge, J. M.; Halpert, J. E.; Wood, V.; Bulovic, V.; Bawendi, M. G. Colloidal Quantum-Dot Light-Emitting Diodes with Metal-Oxide Charge Transport Layers. *Nat. Photonics* **2008**, *2*, 247–250.
23. Zhao, J.; Bardecker, J. A.; Munro, A. M.; Liu, M. S.; Niu, Y.; Ding, I. K.; Luo, J.; Chen, B.; Jen, A. K. Y.; Ginger, D. S. Efficient CdSe/CdS Quantum Dot Light-Emitting Diodes Using a Thermally Polymerized Hole Transport Layer. *Nano Lett.* **2006**, *6*, 463–467.
24. Pal, B. N.; Ghosh, Y.; Brovelli, S.; Laocharoensuk, R.; Klimov, V. I.; Hollingsworth, J. A.; Htoon, H. 'Giant' CdSe/CdS Core/Shell Nanocrystal Quantum Dots As Efficient Electroluminescent Materials: Strong Influence of Shell Thickness on Light-Emitting Diode Performance. *Nano Lett.* **2012**, *12*, 331–336.
25. Bae, W. K.; Park, Y.-S.; Lim, J.; Lee, D.; Padilha, L. A.; McDaniel, H.; Robel, I.; Lee, C.; Pietryga, J. M.; Klimov, V. I. Controlling the Influence of Auger Recombination on the Performance of Quantum-Dot Light-Emitting Diodes. *Nat. Commun.* **2013**, *4*, 2661.
26. Michler, P.; Imamoglu, A.; Mason, M. D.; Carson, P. J.; Strouse, G. F.; Buratto, S. K. Quantum Correlation Among Photons from a Single Quantum Dot at Room Temperature. *Nature* **2000**, *406*, 968–970.
27. Fisher, B.; Caruge, J. M.; Zehnder, D.; Bawendi, M. Room-Temperature Ordered Photon Emission from Multiexciton States in Single CdSe Core-Shell Nanocrystals. *Phys. Rev. Lett.* **2005**, *94*, 087403.
28. Brokmann, X.; Giacobino, E.; Dahan, M.; Hermier, J. P. Highly Efficient Triggered Emission of Single Photons by Colloidal CdSe/ZnS Nanocrystals. *Appl. Phys. Lett.* **2004**, *85*, 712–714.
29. Zavelani-Rossi, M.; Lupo, M. G.; Krahne, R.; Manna, L.; Lanzani, G. Lasing in Self-assembled Microcavities of CdSe/CdS Core/Shell Colloidal Quantum Rods. *Nanoscale* **2010**, *2*, 931–935.
30. Grim, J. Q.; Christodoulou, S.; Di Stasio, F.; Krahne, R.; Cingolani, R.; Manna, L.; Moreels, I. Continuous-wave Biexciton Lasing at Room Temperature Using Solution-Processed Quantum Wells. *Nat. Nanotechnol.* **2014**, *9*, 891–895.
31. She, C.; Fedin, I.; Dolzhnikov, D. S.; Demortière, A.; Schaller, R. D.; Pelton, M.; Talapin, D. V. Low-Threshold Stimulated Emission Using Colloidal Quantum Wells. *Nano Lett.* **2014**, *14*, 2772–2777.
32. Robel, I.; Gresback, R.; Kortshagen, U.; Schaller, R. D.; Klimov, V. I. Universal Size-Dependent Trend in Auger Recombination in Direct-Gap and Indirect-Gap Semiconductor Nanocrystals. *Phys. Rev. Lett.* **2009**, *102*, 177404.
33. Htoon, H.; Hollingsworth, J. A.; Dickerson, R.; Klimov, V. I. Effect of Zero- to One-Dimensional Transformation on Multiparticle Auger Recombination in Semiconductor Quantum Rods. *Phys. Rev. Lett.* **2003**, *91*, 227401.
34. Klimov, V. I.; Mikhailovsky, A. A.; McBranch, D. W.; Leatherdale, C. A.; Bawendi, M. G. Quantization of Multiparticle Auger Rates in Semiconductor Quantum Dots. *Science* **2000**, *287*, 1011–1013.
35. Klimov, V. I.; Mikhailovsky, A. A.; Xu, S.; Malko, A.; Hollingsworth, J. A.; Leatherdale, C. A.; Eisler, H.-J.; Bawendi, M. G. Optical Gain and Stimulated Emission in Nanocrystal Quantum Dots. *Science* **2000**, *290*, 314–317.

36. Schäfer, J.; Mondia, J. P.; Sharma, R.; Lu, Z. H.; Susha, A. S.; Rogach, A. L.; Wang, L. J. Quantum Dot Microdrop Laser. *Nano Lett.* **2008**, *8*, 1709–1712.
37. Min, B.; Kim, S.; Okamoto, K.; Yang, L.; Scherer, A.; Atwater, H.; Vahala, K. Ultralow Threshold On-Chip Microcavity Nanocrystal Quantum Dot Lasers. *Appl. Phys. Lett.* **2006**, *89*, 191124.
38. Klimov, V. I.; Ivanov, S. A.; Nanda, J.; Achermann, M.; Bezel, I.; McGuire, J. A.; Piryatinski, A. Single-Exciton Optical Gain in Semiconductor Nanocrystals. *Nature* **2007**, *447*, 441–446.
39. Bachelard, N.; Gigan, S.; Noblin, X.; Sebbah, P. Adaptive Pumping for Spectral Control of Random Lasers. *Nat. Phys.* **2014**, *10*, 426–431.
40. Hisch, T.; Liertzer, M.; Pogany, D.; Mintert, F.; Rotter, S. Pump-Controlled Directional Light Emission from Random Lasers. *Phys. Rev. Lett.* **2013**, *111*, 023902.
41. Cao, H.; Zhao, Y. G.; Ho, S. T.; Seelig, E. W.; Wang, Q. H.; Chang, R. P. H. Random Laser Action in Semiconductor Powder. *Phys. Rev. Lett.* **1999**, *82*, 2278–2281.
42. Cao, H.; Xu, J. Y.; Zhang, D. Z.; Chang, S. H.; Ho, S. T.; Seelig, E. W.; Liu, X.; Chang, R. P. H. Spatial Confinement of Laser Light in Active Random Media. *Phys. Rev. Lett.* **2000**, *84*, 5584–5587.
43. Wiersma, D. S. The Physics and Applications of Random Lasers. *Nat. Phys.* **2008**, *4*, 359–367.
44. Türeci, H. E.; Ge, L.; Rotter, S.; Stone, A. D. Strong Interactions in Multimode Random Lasers. *Science* **2008**, *320*, 643–646.
45. Wiersma, D. Laser physics: The Smallest Random Laser. *Nature* **2000**, *406*, 132–135.
46. Turitsyn, S. K.; Babin, S. A.; El-Taher, A. E.; Harper, P.; Churkin, D. V.; Kablukov, S. I.; Ania-Castanon, J. D.; Karalekas, V.; Podivilov, E. V. Random Distributed Feedback Fibre Laser. *Nat. Photonics* **2010**, *4*, 231–235.
47. Wiersma, D. S.; Cavalieri, S. Light Emission: A Temperature-Tunable Random Laser. *Nature* **2001**, *414*, 708–709.
48. Fallert, J.; Dietz, R. J. B.; Sartor, J.; Schneider, D.; Klingshirn, C.; Kalt, H. Co-existence of Strongly and Weakly Localized Random Laser Modes. *Nat. Photonics* **2009**, *3*, 279–282.
49. Gottardo, S.; Sapienza, R.; Garcia, P. D.; Blanco, A.; Wiersma, D. S.; Lopez, C. Resonance-driven Random Lasing. *Nat. Photonics* **2008**, *2*, 429–432.
50. Redding, B.; Choma, M. A.; Cao, H. Speckle-free Laser Imaging Using Random Laser Illumination. *Nat. Photonics* **2012**, *6*, 355–359.
51. Tulek, A.; Polson, R. C.; Vardeny, Z. V. Naturally Occurring Resonators in Random Lasing of π-conjugated Polymer Films. *Nat. Phys.* **2010**, *6*, 303–310.
52. Fotiadi, A. A. Random lasers: An Incoherent Fibre Laser. *Nat. Photonics* **2010**, *4*, 204–205.
53. Rotter, S. Random Lasers: Playing Pinball with Light. *Nat. Phys.* **2014**, *10*, 412–413.
54. Chen, Y.; Herrnsdorf, J.; Guilhabert, B.; Zhang, Y.; Watson, I. M.; Gu, E.; Laurand, N.; Dawson, M. D. Colloidal Quantum Dot Random Laser. *Opt. Express* **2011**, *19*, 2996–3003.
55. Shaklee, K. L.; Leheny, R. F. Direct Determination of Optical Gain In Semiconductor Crystals. *Appl. Phys. Lett.* **1971**, *18*, 475–477.
56. Cihan, A. F.; Kelestemur, Y.; Guzelturk, B.; Yerli, O.; Kurum, U.; Yaglioglu, H. G.; Elmali, A.; Demir, H. V. Attractive versus Repulsive Excitonic Interactions of Colloidal Quantum Dots Control Blue- to Red-Shifting (and Non-shifting) Amplified Spontaneous Emission. *J. Phys. Chem. Lett.* **2013**, *4*, 4146–4152.
57. Dennis, A. M.; Mangum, B. D.; Piryatinski, A.; Park, Y.-S.; Hannah, D. C.; Casson, J. L.; Williams, D. J.; Schaller, R. D.; Htoon, H.; Hollingsworth, J. A. Suppressed Blinking and Auger Recombination in Near-Infrared Type-II InP/CdS Nanocrystal Quantum Dots. *Nano Lett.* **2012**, *12*, 5545–5551.
58. Dorfs, D.; Franzl, T.; Osovsky, R.; Brumer, M.; Lifshitz, E.; Klar, T. A.; Eychmüller, A. Type-I and Type-II Nanoscale Heterostructures Based on CdTe Nanocrystals: A Comparative Study. *Small* **2008**, *4*, 1148–1152.
59. Smith, A. M.; Mohs, A. M.; Nie, S. Tuning the optical and electronic properties of colloidal nanocrystals by lattice strain. *Nat. Nanotechnol.* **2009**, *4*, 56–63.
60. Nakamura, T.; Hosaka, T.; Adachi, S. Gold-nanoparticle-assisted Random Lasing from Powdered GaN. *Opt. Express* **2011**, *19*, 467–475.
61. Popov, O.; Zilbershtein, A.; Davidov, D. Random Lasing from Dye-gold Nanoparticles in Polymer Films: Enhanced Gain at the Surface-plasmon-resonance Wavelength. *Appl. Phys. Lett.* **2006**, *89*, 191116.
62. Hrelescu, C.; Sau, T. K.; Rogach, A. L.; Jäckel, F.; Feldmann, J. Single Gold Nanostars Enhance Raman Scattering. *Appl. Phys. Lett.* **2009**, *94*, 153113.
63. van der Molen, K. L.; Tjerkstra, R. W.; Mosk, A. P.; Lagendijk, A. Spatial Extent of Random Laser Modes. *Phys. Rev. Lett.* **2007**, *98*, 143901.
64. Kalusniak, s.; Wünsche, H. J.; Henneberger, F. Random Semiconductor Lasers: Scattered versus Fabry-Perot Feedback. *Phys. Rev. Lett.* **2011**, *106*, 013901.
65. Chen, O.; Chen, X.; Yang, Y.; Lynch, J.; Wu, H.; Zhuang, J.; Cao, Y. C. Synthesis of Metal-Selenide Nanocrystals Using Selenium Dioxide as the Selenium Precursor. *Angew. Chem., Int. Ed.* **2008**, *47*, 8638–8641.
66. Jasieniak, J.; Smith, L.; Embden, J. v.; Mulvaney, P.; Califano, M. Re-examination of the Size-Dependent Absorption Properties of CdSe Quantum Dots. *J. Phys. Chem. C* **2009**, *113*, 19468–19474.
67. Liu, M.; Guyot-Sionnest, P. Mechanism of Silver(I)-Assisted Growth of Gold Nanorods and Bipyramids. *J. Phys. Chem. B* **2005**, *109*, 22192–22200.
68. Rath, T.; Kunert, B.; Resel, R.; Fritz-Popovski, G.; Saf, R.; Trimmel, G. Investigation of Primary Crystallite Sizes in Nanocrystalline ZnS Powders: Comparison of Microwave Assisted with Conventional Synthesis Routes. *Inorg. Chem.* **2008**, *47*, 3014–3022.
69. Fritz, G.; Glatter, O. Structure and Interaction in Dense Colloidal Systems: Evaluation of Scattering Data by the Generalized Indirect Fourier Transformation Method. *J. Phys.: Condens. Matter* **2006**, *18*, S2403–S2419.